Atmos. Chem. Phys., 13, 4253–4263, 2013
www.atmos-chem-phys.net/13/4253/2013/
doi:10.5194/acp-13-4253-2013

Atmospheric Chemistry and Physics Open Access

Stratospheric loss and atmospheric lifetimes of CFC-11 and CFC-12 derived from satellite observations

K. Minschwaner[1], L. Hoffmann[2], A. Brown[3], M. Riese[4], R. Müller[4], and P. F. Bernath[3,5]

[1]Department of Physics, New Mexico Institute of Mining and Technology, Socorro, NM, USA
[2]Jülich Supercomputing Centre (JSC), Forschungszentrum Jülich, Germany
[3]Department of Chemistry, University of York, UK
[4]Institute of Energy and Climate Research (IEK-7), Forschungszentrum Jülich, Germany
[5]Department of Chemistry and Biochemistry, Old Dominion University, Norfolk, VA, USA

Correspondence to: K. Minschwaner (krm@nmt.edu)

Received: 22 September 2012 – Published in Atmos. Chem. Phys. Discuss.: 5 November 2012
Revised: 15 March 2013 – Accepted: 26 March 2013 – Published: 24 April 2013

Abstract. The lifetimes of CFC-11 and CFC-12 have been evaluated using global observations of their stratospheric distributions from satellite-based instruments over the time period from 1992 to 2010. The chlorofluorocarbon (CFC) datasets are from the Cryogen Limb Array Etalon Spectrometer (CLAES), the Cryogenic Infrared Spectrometers and Telescopes for the Atmosphere (CRISTA-1 and CRISTA-2), the Michelson Interferometer for Passive Atmospheric Sounding (MIPAS), and the Atmospheric Chemistry Experiment (ACE). Stratospheric loss rates were calculated using an ultraviolet radiative transfer code with updated cross section and solar irradiance data. Mean steady-state lifetimes based on these observations are 44.7 (36–58) yr for CFC-11 and 106.6 (90–130) yr for CFC-12, which are in good agreement with the most recent WMO ozone assessment. There are two major sources of error in calculating lifetimes using this method. The first important error arises from uncertainties in tropical stratospheric observations, particularly for CFC-11. Another large contribution to the error is due to uncertainties in the penetration of solar ultraviolet radiation at wavelengths between 185 and 220 nm, primarily in the tropical stratosphere between 20 and 35 km altitude.

1 Introduction

Atmospheric lifetimes for chlorofluorocarbons (CFCs) are important for interpreting their observed atmospheric distributions, temporal trends, and for evaluating their impact on stratospheric chemistry and infrared radiative forcing. There are a variety of techniques available for estimating CFC lifetimes. Atmospheric models can be used to evaluate trace gas lifetimes in a self-consistent fashion by calculating the emissions, transport, and chemical sources and sinks to simulate global trace gas distributions (e.g., Douglass et al., 2008). Alternatively, measurements of CFCs can be used to calculate their lifetimes. Observationally based techniques include inverse methods used in conjunction with emission estimates (e.g., Cunnold et al., 1983), calculations of loss rates associated with global climatologies (e.g., Minschwaner et al., 1998), and the use of observed tracer-tracer correlations (e.g., Plumb and Ko, 1992; Volk et al., 1997).

The study by Johnston et al. (1979) of nitrous oxide (N_2O) was one of the first to use global measurements in combination with modeled photolytic loss rates to examine the distribution of stratospheric loss for a long-lived gas, and to assess its lifetime. This early work utilized a global N_2O climatology based on aircraft, balloon, and rocket measurements of stratospheric vertical profiles spanning a range of latitudes. One aspect of this approach, in comparison to lifetimes based on 2- or 3-D model simulations, is that the trace gas distribution could be constrained without the need for a detailed analysis of winds, mixing, dynamical parameterizations, and uncertainties associated with trace gas transport.

Subsequent work by Crutzen and Schmailzl (1983), Ko et al. (1991), and Minschwaner et al. (1993) incorporated the use of global N_2O data from the Stratospheric and Mesospheric Sounder (SAMS) instrument on the Nimbus 7

satellite. The availability of higher precision global data and a wider array of species from the Upper Atmosphere Research Satellite (UARS) led to a reevaluation of N_2O and CFC-12 (CF_2Cl_2) loss, and produced steady-state lifetime estimates of 117 ± 26 yr for N_2O and 103 ± 25 yr for CFC-12 (Minschwaner et al., 1998).

The lifetime of CFC-11 ($CFCl_3$) has been estimated from model calculations, and from observations made from aircraft and balloon platforms. One of the first 1-D modeling calculations (Wofsy et al., 1975) yielded an estimate of 45 yr. Later simulations with higher-dimensional models produced longer lifetimes, with a range between 47 yr and 74 yr (Ko and Sze, 1982; Jackman and Guthrie, 1985; Cunnold et al., 1986). The use of balloon- and aircraft-based climatologies yielded a shorter lifetime estimate of 41.5 ± 12.5 yr (Minschwaner et al., 1993), while analysis of lower stratospheric vertical gradients and age-of-air estimates from aircraft measurements produced a similar value of 41 ± 12 yr (Volk et al., 1997). Most recently, Douglass et al. (2008) found that model simulations with realistic age-of-air diagnostics suggested a longer lifetime of 56–64 yr, outside of the range of observationally based CFC-11 lifetimes. Constraints from satellite measurements have not yet been applied to this problem.

Revisions in the CFC-11 lifetime would affect estimates of its global emission inventories derived from changes in atmospheric concentrations. Changes to this lifetime would also impact the assessment of the potential of CFC-11 for destroying stratospheric ozone (the so-called ozone depletion potential (ODP)), and thus predictions of the recovery of the ozone layer (e.g., Newman et al., 2007). Since the ODP for many other compounds is calculated relative to CFC-11, this would also force changes in calculated values for many ODPs. Furthermore, best-estimate lifetimes for other halocarbons, which have been derived relative to CFC-11 by means of tracer-tracer correlations, would be affected.

In this paper, new results are presented for CFC lifetimes from global CFC-11 and CFC-12 distributions based on satellite-based measurements spanning the years 1992–2010: CFC-12 from the Cryogen Limb Array Etalon Spectrometer (CLAES) (Nightingale et al., 1996), CFC-11 from the Cryogenic Infrared Spectrometers and Telescopes for the Atmosphere (CRISTA-1 and CRISTA-2) (Riese et al., 1999; Kuell et al., 2005), both CFC molecules from the Michelson Interferometer for Passive Atmospheric Sounding instrument (MIPAS) (Hoffmann et al., 2005, 2008), and both CFC molecules from the Atmospheric Chemistry Experiment (ACE) (Bernath et al.,2005; Brown et al., 2011).

2 CFC photolysis rates

In this section we present a detailed examination of the photodissociation of CFC-11 and CFC-12 in order to identify key quantities and related uncertainties that impact the calculation of CFC lifetimes. It will be shown that the penetration of solar ultraviolet radiation in the 20–35 km altitude range is an important consideration for this work. The expression for the photolysis rate of a given molecule (Brasseur and Solomon, 2005), neglecting scattering and assuming a quantum yield of unity, is

$$J(z) = \int I_\lambda \, \sigma_\lambda(z) \exp[-\tau_\lambda(z) \sec\vartheta] \, d\lambda, \quad (1)$$

where I_λ is the solar spectral irradiance, σ_λ the absorption cross section for the molecule of interest, and τ_λ is the atmospheric vertical optical depth. All of these quantities are functions of wavelength, λ, and the optical depth and absorption cross section are also functions of altitude, z (the latter through the temperature dependence of cross sections). The factor $\sec\vartheta$, where ϑ is the solar zenith angle, accounts for slant-path opacity through the overhead atmospheric column.

Absorption cross sections for CFC-12 and CFC-11 have maximum values at wavelengths between 175 and 180 nm, but atmospheric opacity due to O_2 at these wavelengths is very large and prevents most of the solar radiation for $\lambda < 185$ nm from reaching the stratosphere. As shown later, the most critical wavelengths for stratospheric photodissociation of CFC-12 and CFC-11 are between 185 and 220 nm. Figure 1 compares CFC cross section measurements from Simon et al. (1988) and Merienne et al. (1990) at 225 K. Both of these measurements indicated a significant dependence on temperature, with reduced cross sections at lower temperatures. For example, CFC-12 cross sections at 200 nm are 36 % smaller at 230 K compared to 295 K (Simon et al., 1988). This effect must be considered in atmospheric calculations since, as shown below, most of the photolytic destruction of the CFCs occurs in the low-latitude stratosphere between 20 and 35 km altitude where temperatures typically range between 210 K and 240 K. Figure 1 also displays results of the temperature-dependent parameterizations from Jet Propulsion Laboratory (JPL) Evaluation 17 (Sander et al., 2011) and from JPL Evaluation 12 (DeMore et al., 1997).

Considering first CFC-12, there is good agreement between the two sets of measurements at 200 nm, but differences grow to about 12 % at 220 nm. Note that, for both molecules, the Merienne et al. (1990) measurements do not extend below 200 nm. The polynomial expression derived by Merienne et al. (1990) and recommended for use in model calculations (Sander et al., 2011) provides an excellent fit for wavelengths above 200 nm. As noted by Sander et al. (2011), this expression is valid for the wavelength range 200–231 nm so that below 200 nm the parameterization grossly overestimates the cross section compared to the Simon et al. (1988) measurements, as seen in Fig. 1. Furthermore, the parameterization reported by Simon et al. (1988) for this wavelength range contained errors making it unsuitable for use in modeling applications. On the other hand, the cross sections with exponential temperature correction recommended by DeMore et al. (1997) provide an excellent fit to the mean of the measurements over the entire wavelength range, and

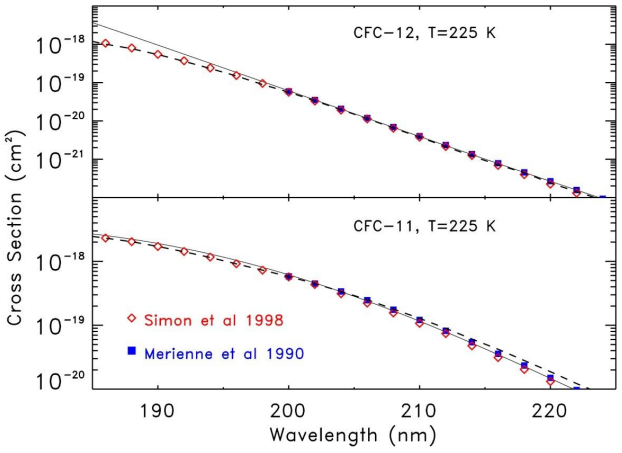

Fig. 1. Absorption cross section measurements interpolated to 225 K from Simon et al. (1988) (red diamonds) and Merienne et al. (1990) (blue squares) for CFC-12 (top) and CFC-11 (bottom). Also plotted are empirical polynomial fits (solid curves) that incorporate the wavelength and temperature dependencies (Sander et al., 2011) along with empirical exponential fits (dashed curves) to temperature-dependent cross sections from DeMore et al. (1997).

we have adopted this formulation for CFC-12. If photolysis calculations are carried out by limiting the parameterized CFC-12 cross sections above 200 nm, or by extrapolating the Merienne et al. (1990) expression below 200 nm, then the resulting J values could be in error by more than 15 %.

For CFC-11, the agreement between the two sets of cross section measurements is similar to that for CFC-12. The polynomial expression derived by Simon et al. (1988) and recommended for use in modeling calculations (Sander et al., 2011) provides a reasonable fit to the measurement mean above 200 nm, but it overestimates the CFC-11 cross section below 200 nm (e.g., by 11 % at 190 nm). On the other hand, the expression recommended by DeMore et al. (1997) provides an excellent fit below 200 nm but overestimates the measurements above 200 nm. We therefore use the Simon et al. (1988) expression above 200 nm and the DeMore et al. (1997) formulation below 200 nm in order to provide an optimum representation of CFC-11 absorption and photolytic destruction.

Photolysis rates for CFC-11 and CFC-12 were calculated using the ultraviolet radiative transfer code described by Minschwaner et al. (1993). This model incorporates a high-resolution, line-by-line treatment of temperature-dependent absorption in the Schumann–Runge (S-R) bands of O_2 in the spectral region 175 to 205 nm. At longer wavelengths up to 242 nm, O_2 absorption cross sections in the weaker Herzberg continuum region are adopted from the measurements of Yoshino et al. (1988). Opacity by ozone is included using cross sections recommended by Sander et al. (2011) and ozone zonal and seasonal mean mixing ratios used by Minschwaner et al. (1998), which were based on Microwave Limb Sounder (MLS) data from the Upper Atmosphere Research Satellite (UARS). Comparisons between this ozone climatology and others derived from UARS instruments (Wang et al., 1999; Grooß and Russell, 2005) indicated a small bias of +3 % in the low-latitude stratosphere in the Minschwaner et al. (1998) climatology (see Appendix A), which has been corrected in the calculations presented here. Temperatures needed for calculating absorption cross sections are from the same UARS climatology. Multiple scattering effects are generally small (< 7 %) at these wavelengths in the stratosphere (Minschwaner, 1994) but are included using the model formulation of Meier et al. (1982). Solar irradiances in the wavelength range from 115 to 420 nm are specified from measurements during March 2004, from the Solar Radiation and Climate Experiment (SORCE) (Rottman et al., 2006). Considering the possibility of solar variability on ultraviolet irradiances, there could be variations of up to ±4 % near 200 nm from solar maximum to solar minimum conditions (Lean, 2000), which would translate directly into changes in photolytic loss and associated lifetimes. The 2004 time period used here represents the approximate mean state of solar activity so that our calculations reflect a time-averaged, steady-state lifetime.

The integrand to Eq. (1), referred to here as the spectral J value, can provide insights into the wavelength regions, sources of opacity, and altitudes that are relevant for determining the overall photolysis rate. Spectral J values for CFC-12 and CFC-11 are displayed in Fig. 2 for pressures of 6, 20, and 60 hPa. In the tropical stratosphere where values in Fig. 2 are most appropriate, the corresponding altitudes are approximately 35, 27, and 20 km, respectively.

The impact of highly structured absorption by the O_2 S-R bands is apparent for $\lambda < 200$ nm in Fig. 2, where much of the photolysis for both molecules occurs in narrow windows between vibrational band absorption features. For wavelengths longer than 210 nm, the contribution to photolysis falls off rapidly due to the increasing shielding from ozone absorption in the Hartley band. This effect is larger for CFC-12 than for CFC-11 due to the more rapid decrease in the CFC-12 cross section with increasing wavelength (Fig. 1), which also shifts the region of maximum spectral J value to shorter wavelengths: for CFC-12 this peak occurs approximately between 190 and 210 nm, whereas for CFC-11 the peak photolysis is in the 195–215 nm wavelength range. Additionally, there is a shift of emphasis to longer wavelengths with increasing pressure for both molecules, which occurs because the ozone optical depth does not grow as rapidly as the oxygen optical path with increasing pressure at altitudes below the peak in ozone mixing ratio. Overall, spectral J values for CFC-12 are about a factor of 2 to 3 smaller than for CFC-11, and this is consistent with the magnitude of the cross sections shown in Fig. 1. Differences of the same magnitude will also be apparent in the lifetimes discussed below.

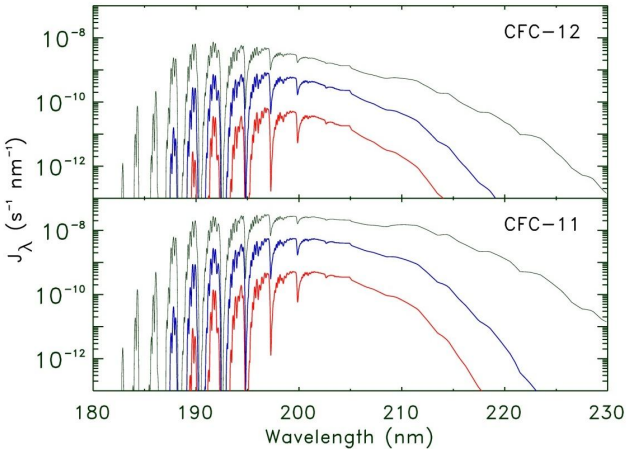

Fig. 2. Spectrally resolved contributions to the photolysis rates for CFC-12 (top) and CFC-11 (bottom) plotted for pressures of 6 hPa (black), 20 hPa (blue), and 60 hPa (red) calculated for the tropical stratosphere using March climatological temperatures and ozone (see text for details) and a solar zenith angle of 30°. Spectral J values below 200 nm have been smoothed at 0.1 nm full width at half maximum for clarity of presentation.

3 Global destruction rates and lifetimes

3.1 General methodology

Transient lifetimes $T(t)$ for the CFCs were calculated from the global atmospheric burden, M, divided by the global loss rate, L, for a given time t:

$$T(t) = \frac{M(t)}{L(t)} \tag{2}$$

where both $M(t)$ and $L(t)$ are determined from the local concentrations of CFC molecules, $n(\varphi, z, t)$, and from photolysis rates $J(\varphi, z, t)$, which are functions of latitude φ, altitude z, and time t. There is also a small ($< 10\,\%$) contribution to global CFC loss due to reaction with excited state atomic oxygen, O(^{1}D). In addition to transient lifetimes that can be calculated directly using observed trace gas distributions, we will later include an evaluation of steady-state lifetimes that are appropriate under conditions where loss and emission rates are in balance.

The quantities M and L in Eq. (2) are global values obtained by integrating over altitude and latitude (assuming zonal symmetry in the distributions of gas concentration and loss):

$$M(t) = 2\pi R_E^2 \int dz \int n(\varphi, z, t) \cos\varphi \, d\varphi \tag{3}$$

$$L(t) = 2\pi R_E^2 \int dz \int n(\varphi, z, t) \left\{ J(\varphi, z, t) + k_1 [O(^1D)(\varphi, z, t)] \right\} \cos\varphi d\varphi, \tag{4}$$

where R_E is the Earth radius, $[O(^1D)(\varphi, z, t)]$ is the concentration of excited state atomic oxygen (which is also a function of latitude, altitude and time), and k_1 is the rate for reaction of O(^{1}D) with CFCs. Values for the rate constant k_1 were taken from Sander et al. (2011), and the distribution of O(^{1}D) was calculated using equilibrium photochemical expressions (Brasseur and Solomon, 2005) involving ozone and the ozone photodissociation rate calculated using the radiative transfer model. For both photolytic and reactive loss with O(^{1}D), diurnally averaged values were calculated by integrating over the range of solar zenith angle conditions appropriate for each latitude and season. Atmospheric burdens are computed using a mean surface pressure of 985 hPa to account for the effects of surface topography. Loss rate integrals are also taken from this mean surface pressure up to 0.1 hPa (near 64 km), although as shown below, over 95 % of the loss for both species occurs in the stratosphere.

3.2 CFC observations

The distributions of CFC-11 and CFC-12 used in Eqs. (3) and (4) were determined from satellite-based measurements. These include global satellite observations of CFC-12 from CLAES between March 1992 and January 1993 (Nightingale et al., 1996), CFC-11 from CRISTA-1 in November 1994 (Riese et al., 1999) and from CRISTA-2 in August 1997 (Kuell et al., 2005), CFC-11 from MIPAS for the period July 2002 to March 2004 and CFC-12 from MIPAS for December 2002 to February 2003 (Hoffmann et al., 2005, 2008), and CFC-11 and CFC-12 from ACE over the period 2006–2010 (Bernath et al., 2005; Brown et al., 2011). Some of these datasets are limited in seasonal or interannual coverage. For example, both CRISTA CFC-11 distributions are based on 8-day observation periods due to the finite duration of space shuttle flights used to deploy both satellite platforms (Offermann et al., 1999; Grossmann et al., 2002). The impact of not accounting for seasonal and interannual variations in CFC distributions is explored below.

Zonal averages for all datasets were linearly interpolated to a 1 km altitude grid from the surface to 50 km, and into latitudinal bins on a 5° grid from 85° S to 85° N. Values above the top of measured profiles were extrapolated to zero using cubic splines with mixing ratios and gradients that matched the data at the uppermost valid measurement. At the bottom of vertical profiles, increasing mixing ratios down to 10 km altitude were linearly extrapolated where necessary to match the global/annual mean tropospheric mixing ratio at the time of each measurement (WMO, 2011). Mixing ratios from 10 km to the surface were held constant at the 10 km value.

For CLAES CFC-12 and MIPAS CFC-11, mean seasonal distributions were constructed based on climatologies for four seasons: December–February, March–May, June–August, and September–November. The MIPAS CFC distributions incorporated adjustments to the altitude scale given

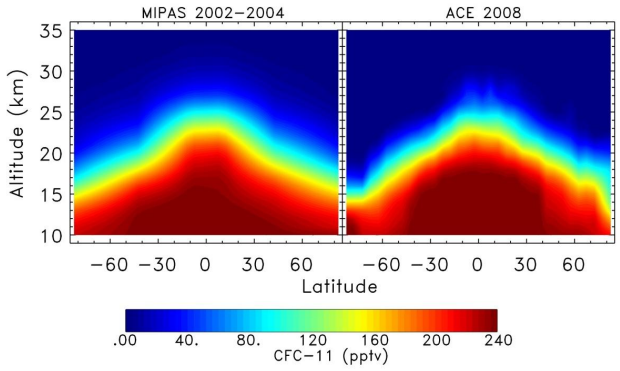

Fig. 3. Zonal mean distributions of CFC-11 from MIPAS averaged over 2002–2004 (left) and from ACE 2008 annual mean (right).

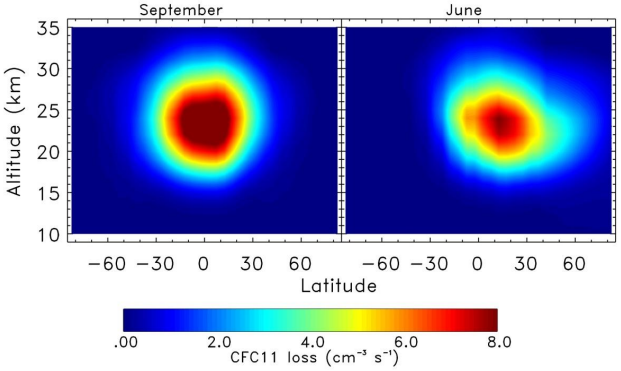

Fig. 4. Loss rate for CFC-11 based on MIPAS distributions for September (left) and for June (right), in units of molecules $cm^{-3}\,s^{-1}$.

in Hoffmann et al. (2008) by calculating geopotential heights using the native pressure grid from the MIPAS retrievals along with the temperature climatology discussed above (Minschwaner et al., 1998). Corrections to the published altitudes were less than +0.5 km below 18 km, and between −0.2 and −1.8 km at greater altitudes. Global fields for ACE CFCs were constructed using one full year of data in order to produce annual means with sufficient coverage at low latitudes. For CRISTA-1 and 2 CFC-11, the data represent means over ±70° latitude for 8-day periods during the months of November and August, respectively.

Figure 3 compares the MIPAS CFC-11 mean distribution for 2002–2004 with the ACE annual mean 2008 climatology. Tropospheric levels of CFC-11 declined by about 4 % over the time between the MIPAS and ACE measurements, which produces differences too small to be discerned in this figure. In general, the two distributions show similar features in the stratosphere. Larger mixing ratios occur in the low-latitude stratosphere due to upwelling of CFC-rich air across the tropical tropopause in the upwelling branch of the Brewer–Dobson circulation. Mixing ratios decrease with increasing altitude in both distributions as a result of photochemical destruction. The largest fractional difference between MIPAS and ACE occurs at high latitudes below about 25 km altitude, although due to the pattern of loss presented below, such differences are not important for the CFC-11 lifetime. At all latitudes but particularly in the tropics, MIPAS mixing ratios are larger by 10–20 % than ACE values above 20 km. At most, 4 % of the difference might be attributed to the decline in tropospheric burden. Thus, it may be concluded that many of the differences in Fig. 3 are real measurement biases between datasets, which can have a significant impact on the calculated lifetimes.

3.3 CFC loss rates

Rates for CFC-11 loss (Eq. 4) derived from MIPAS data for equinox and solstice are shown in Fig. 4. Consistent with previous observationally based studies (Minschwaner et al., 1993) and model results (Douglas et al., 2008), CFC-11 destruction is largest in the low-latitude stratosphere between 20 and 28 km altitude. Globally integrated rates are dependent on season; average loss rates are 12 % larger during the equinoxes as compared to the solstices. The main drivers of this variation are the seasonal changes in sun angle, ozone, and CFC-11 mixing ratios. The largest impact is due to smaller solar zenith angles at low latitudes during equinox, with associated increases in actinic fluxes and photolytic destruction in the low-latitude stratosphere. Changes in ozone act to reinforce the seasonal variation, with smaller mixing ratios in March than in June, which leads to greater penetration of solar radiation in March. Changes in MIPAS CFC-11 mixing ratios play a minor role in seasonal loss variations (about 5 %). With larger mixing ratios during the solstices, these CFC-11 seasonal variations act to oppose the impact of changes in actinic flux on the CFC-11 loss rate. The year-to-year variability in annual mean loss rate from the ACE dataset is between 5 % and 10 %, which provides a rough measure of interannual variability caused by phenomena such as the quasi-biennial oscillation.

The distribution of CFC-12 loss is shown in Fig. 5 for ACE 2008 annual mean data and equinox solar conditions. In addition, the fraction of this loss resulting from reaction with $O(^1D)$ is displayed. Comparison of Figs. 4 and 5 shows that both CFC loss rates are largest in the tropical lower and mid-stratosphere, but CFC-12 destruction is shifted upward about 6 km relative to CFC-11. Also, CFC-12 loss rates are 30–40 % smaller than for CFC-11, which, along with a larger global burden, translates into a longer lifetime for CFC-12 compared with CFC-11. Reaction with $O(^1D)$ dominates the total loss below 12 km and in the lower stratosphere at high latitudes, but these regions have a negligible impact on the global loss. Where CFC-12 loss rates are largest (the tropical stratosphere between 26 and 34 km), reaction with $O(^1D)$ accounts for 4–8 % of the total loss. The $O(^1D)$ contribution

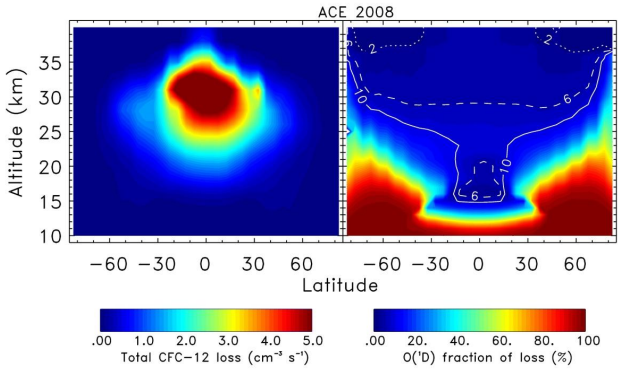

Fig. 5. Loss rate for CFC-12 based on ACE 2008 annual mean data and March distributions of ozone, temperature, and solar conditions (left), along with the fraction of the total loss that results from reaction with $O(^1D)$ for the same CFC-12 and atmospheric conditions (right). Contours are indicated on the right plot for 2 % (dotted), 6 % (dashed), and 10 % (solid) fraction of $O(^1D)$ loss.

to CFC-11 loss (not shown) has a similar distribution and magnitude; thus the global loss of both CFCs is governed primarily by direct photodissociation.

3.4 CFC lifetimes

Table 1 lists the CFC-11 datasets, observation time periods, global mean loss rates and burdens, and the transient and steady-state lifetimes derived from the measurements. All loss rates and burdens are based on calculated means over four seasonal values. Results for CRISTA-1 and CRISTA-2 employed a constant CFC-11 distribution over all seasons, and ACE values are based on 4 yr averages of loss rates derived from the annual mean CFC-11 distributions. The use of observations from a single season or year may introduce some bias error in connection with seasonal or interannual variability in trace gas mixing ratios. Based on MIPAS CFC-11 and CLAES CFC-12 measurements where sufficient seasonal coverage is available, seasonal changes in their distributions can impact computed loss rates by up to 5 % and 7 %, respectively. Interannual effects on computed lifetimes, based on the year-to-year variability of ACE results, are 5–10 % for both CFC-11 and CFC-12. Table 1 also provides uncertainties in steady-state lifetimes based on a detailed analysis of multiple sources of error (see Appendix A). Uncertainties in transient lifetimes are not listed but are similar in magnitude. The fractional lifetime error for each dataset is on the order of 30–40 %, and errors are asymmetric because the uncertainties are dominated by loss rate uncertainties, which appear in the denominator of the lifetime expression (Eq. 2).

Steady-state lifetimes were derived from transient lifetimes using a simple linear growth correction. In steady state, CFC emissions to the atmosphere exactly balance stratospheric loss and the mean tropospheric concentration is constant. If there is an imbalance between sources and sinks, however, then the mean tropospheric concentration will change with time, and the transient lifetime based on instantaneous stratospheric loss will differ from the steady-state lifetime. This difference is due to the finite time lag between temporal changes in abundances for the stratosphere relative to the troposphere (approximately given by the "mean age" of air). We applied a scaling factor, S, to the transient lifetime to approximate this difference:

$$S = \left(1 + \frac{1}{\bar{n}} \frac{\mathrm{d}\bar{n}}{\mathrm{d}t} \Delta t\right)^{\frac{\Gamma}{\Delta t}}, \quad (5)$$

where $\mathrm{d}\bar{n}/\mathrm{d}t$ is the mean tropospheric growth or decay rate, and Γ is the mean age of air in the stratosphere near the region of maximum loss. We use a time step Δt of one year so that $100\left(1/\bar{n}\right)\mathrm{d}\bar{n}/\mathrm{d}t$ is expressed in units of % yr^{-1} and Γ is in units of yr. Since S represents a correction to steady state for stratospheric concentrations used in calculating CFC loss, transient lifetimes are multiplied by $1/S$ to obtain steady-state lifetimes.

For CFC-11, decreases in global mean tropospheric abundances during 1997–2010 were between $-0.5\,\%\,\mathrm{yr}^{-1}$ and $-1\,\%\,\mathrm{yr}^{-1}$ (WMO, 2011) indicating a larger stratospheric loss relative to tropospheric emissions. Assuming a mean time lag of 2 yr for air to ascend through the tropical tropopause to 30 km altitude (Schoeberl et al., 2008), steady-state lifetimes are 1 % to 2 % longer than transient lifetimes for the CRISTA-2, MIPAS, and ACE distributions. For CRISTA-1, 1994 marks the approximate peak in tropospheric mixing ratio, and therefore the steady-state lifetime is nearly identical to the computed transient lifetime.

The best-estimate lifetime shown in Table 1 is calculated from the inverse mean of the individual $1/T$ values. It is calculated in $1/T$ space to account for the primary difference between values that arises from the CFC distributions appearing in the denominator of the expression for T (Eqs. 3 and 4). Furthermore, since the two CRISTA CFC-11 results were obtained from the same instrument with similar retrievals, these inverse lifetimes were averaged prior to calculating the mean. No other weighting has been applied to compute the best estimate. Considering the large number of profiles that were used in all of the datasets, differences in statistical errors are not important, and estimated systematic uncertainties are not considerably different between instruments. Seasonal sampling issues discussed above could impact results, but these were judged to be too small to justify any weighting based on season. The best-estimate CFC-11 steady-state lifetime is 44.7 yr, with a 1-σ uncertainty range between 36 and 58 yr.

The large spread in lifetimes derived from the four measurements (24.6 yr from minimum to maximum) results primarily from differences in low-latitude mixing ratios between 20 and 28 km altitude. This range in lifetime is also consistent with the estimated uncertainties due to stratospheric concentrations (about $\pm$11 yr; see Appendix A). Figure 6 compares tropical mean stratospheric mixing ratios of

Table 1. CFC-11 lifetimes based on global satellite observations.

Instrument	Observation Period Used	Mean Global Burden (10^{34} molecules)	Mean Loss Rate (10^{25} molecules s^{-1})	Transient Lifetime (yr)	Steady-State Lifetime (yr)
CRISTA-1	Nov 1994	2.71	1.63	52.7	52.9 (41–75)
CRISTA-2	Aug 1997	2.64	1.39	60.0	60.7 (47–86)
MIPAS	2002–2004	2.50	2.24	35.4	36.1 (28–50)
ACE	2006–2010	2.38	1.67	45.2	46.1 (36–65)
Best Estimate					44.7 (36–58)

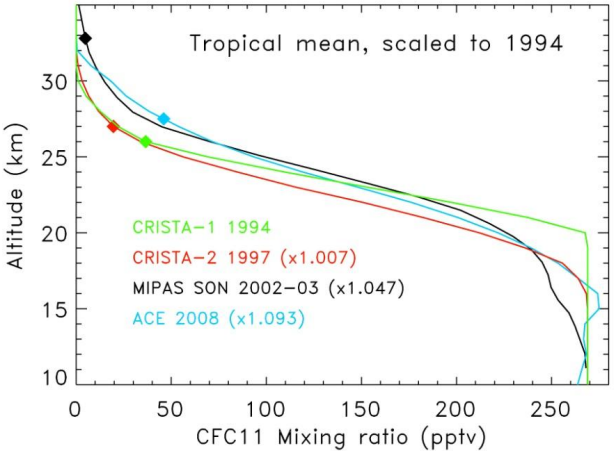

Fig. 6. Tropical mean vertical profiles of CFC-11 mixing ratio from CRISTA-1 (green), CRISTA-2 (red), MIPAS (black), and ACE (blue), all scaled to a tropospheric mean mixing ratio of 269 ppt using altitude-independent factors for comparison. Scaling factors are given in the figure legend. Diamond symbols represent the mean top of measured profiles for each instrument; profiles above these levels are cubic spline extrapolations to zero mixing ratios as described in the text.

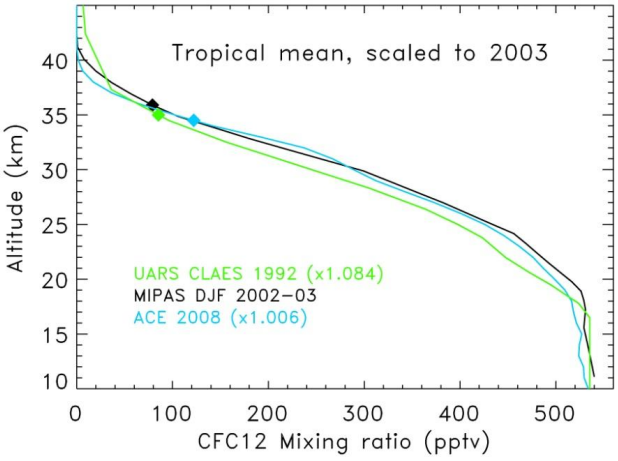

Fig. 7. Same as Fig. 6, but plotted are tropical mean vertical profiles of CFC-12 mixing ratio from UARS CLAES (green), MIPAS (black), and ACE (blue), all scaled to a tropospheric mean mixing ratio of 542 ppt using altitude-independent factors.

CFC-11 from the four satellite datasets used in our analysis. During the period of interest, tropospheric CFC-11 mixing ratios peaked around 1994, and all profiles were uniformly scaled to match the 1994 mean tropospheric mixing ratio. The use of an altitude-independent scaling may cause differences of up to 2 % in stratospheric mixing ratios because of non-steady-state conditions and time lags for changes in the troposphere to appear in the stratosphere. However, differences between values for the satellite data are much larger at 25 km, near the altitude of peak CFC-11 loss. The minimum mixing ratio at 25 km is 56 ppt from CRISTA-2 while the maximum is 100 ppt from MIPAS. This broad range is reflected in the CFC-11 loss rates, which are smallest for CRISTA-2 and largest for MIPAS data. Likewise, the derived CFC-11 steady-state lifetimes range from 60.7 yr for the CRISTA-2 climatology to 36.1 yr for the MIPAS climatology. It should be noted that comparisons between the satellite CFC-11 climatologies, and also between satellite and in situ balloon measurements, are complicated by the extremely large vertical gradient in mixing ratio such that small altitude shifts of 1 km or less can have a dramatic impact (Appendix A).

Table 2 lists the CFC-12 loss rates, burdens, and lifetimes derived from the three sets of measurements. CFC-12 abundances in the troposphere peaked around 2002–2003, and we have assumed growth rates of $+2\,\%\,yr^{-1}$ for CLAES, zero for MIPAS, and $-0.5\,\%\,yr^{-1}$ for ACE, along with a mean age of 2.5 yr at 30–35 km in the tropics in order to derive steady-state lifetimes. As indicated in Table 2, the variation between datasets for the CFC-12 steady-state lifetime is much smaller than for CFC-11, with a max-min spread of only 3.5 yr. This level of agreement is remarkable given the typical uncertainty of 20–28 yr due to stratospheric profile error sources. It should be noted that the reanalysis of CLAES CFC-12 data presented here includes revisions to the absorption cross section and ozone opacity in comparison to Minschwaner et al. (1998), leading to a difference of about 5 yr in the derived lifetime. The best-estimate, CFC-12 steady-state lifetime is 106.6 yr, with a 1-σ uncertainty range of 90 to 130 yr.

Table 2. CFC-12 lifetimes based on global satellite observations.

Instrument	Observation Period Used	Mean Global Burden (10^{34} molecules)	Mean Loss Rate (10^{25} molecules s^{-1})	Transient Lifetime (yr)	Steady-State Lifetime (yr)
CLAES	1992–1993	5.00	1.40	113.3	108.0 (88–140)
MIPAS	2002–2003	5.50	1.62	107.5	107.5 (83–151)
ACE	2006–2010	5.31	1.63	103.3	104.5 (84–139)
Best Estimate					106.6 (90–130)

Figure 7 compares tropical profiles from the three CFC-12 satellite datasets used to derive the lifetimes listed in Table 2. In contrast to CFC-11, there is better agreement between measured CFC-12 vertical profiles in the tropical stratosphere, which leads to the smaller range in derived lifetimes. At 31 km near the altitude of peak CFC-12 loss, mixing ratios range from 210 ppt from CLAES to about 250 ppt from MIPAS and ACE. Differences become even smaller at higher altitudes (e.g., less than 15 % spread at 35 km).

4 Discussion and conclusion

Best-estimate, steady-state lifetimes derived here (44.7 (36–58) yr for CFC-11 and 106.6 (90–130) yr for CFC-12) are in good agreement with the most recent WMO ozone assessment recommendations (45 yr for CFC-11 and 100 yr for CFC-12) (WMO, 2011). The CFC-11 lifetime is not consistent with the longer lifetime suggested by Douglass et al. (2008), although their range of 56–64 yr overlaps with the upper end of our value. In the case of CFC-12, our steady-state lifetime is about 6 % longer than the WMO recommendation, but this difference is well within our uncertainty range.

The major contrasts between CFC-11 and CFC-12 in our analysis arise from differences in the absorption cross sections and from differences in stratospheric vertical profiles, most notably within the tropical stratosphere below 35 km altitude. These two issues are related since, for similar upward transport rates in the tropical stratosphere, larger cross sections for CFC-11 lead to more rapid destruction and a sharper decline in mixing ratio with height relative to CFC-12. In fact, a major difficulty in calculating CFC-11 destruction relates to the very large vertical gradient in mixing ratio. This large gradient complicates space-based observations, which may have extended vertical fields of view, averaging kernels, or uncertainties in absolute altitude registration, and small errors in any of these quantities are magnified in calculated loss rates.

In addition to uncertainties associated with observed CFC profiles, another major source of error in these calculations is associated with the penetration of ultraviolet solar radiation between 20 and 35 km altitudes within the tropical stratosphere. Uncertainties in oxygen and ozone opacities are both critical factors; the former is caused by uncertainties in oxygen absorption cross sections, whereas the latter is dominated by measurement uncertainties and variability in the tropical ozone distribution. Despite some progress in constraining the oxygen absorption cross section from laboratory measurements over the past two decades, there have been very few in situ measurements of the spectrally resolved radiation field in the 190–215 nm spectral region, where such wavelengths are critical for CFC photodissociation. Measurements in the tropical stratosphere would be particularly valuable for obtaining more accurate estimates of CFC lifetimes.

Appendix A

Error analysis

There are multiple sources of error for the CFC lifetimes that arise from uncertainties in the terms appearing in the loss rate calculation (Eq. 4). The primary uncertainties are related to the climatologies of stratospheric CFC concentrations and to calculated photolysis rates. Table A1 contains a breakdown of the uncertainties for both CFC-11 and CFC-12. All of the errors considered here are taken at the 1-σ level.

Stratospheric concentration uncertainties originate from many effects, but the dominant terms are measurement random and systematic errors, uncertainties in altitude, and the smoothing effect of vertical resolution. These vary considerably among the different measurements. Uncertainties may also vary depending on latitude, altitude, and season. The range of years given in Table A1 reflect the combined effects based on sensitivity calculations designed to investigate altitude shifts and impacts of averaging kernels on computed lifetimes. For example, we found that a uniform 1 km shift to CFC-11 profiles produced a net change of 24 % in CFC-11 loss rates; the impact of such a shift on CFC-12 was much less (15 %) due to its much smaller vertical gradient. Similarly, the impact of vertical smoothing due to averaging kernels used in retrievals could be as large as 10 % for CFC-11 loss but only 6 % for CFC-12, with both loss rates increased due to tendencies for larger mixing ratios on the top side of profiles as a consequence of smoothing. For both CRISTA datasets and MIPAS profiles, estimated uncertainties in geometric or log-pressure altitude are 0.3–0.5 km, and

Table A1. Contributions to CFC lifetime uncertainties (yr).

	CFC-11	CFC-12
Stratospheric concentrations	7.2–13.3	20.2–28.0
Solar spectral irradiances	1.4–2.4	4.2
CFC cross sections	1.8–3.0	5.2–5.4
Oxygen opacity	6.2–10.4	10.2–10.5
Ozone opacity	2.9–4.8	4.7–4.8
$O(^1D)$ loss	0.4–0.6	1.1
Global burden	0.6–0.9	1.6
Steady-state conversion	0.6	1.4–1.8

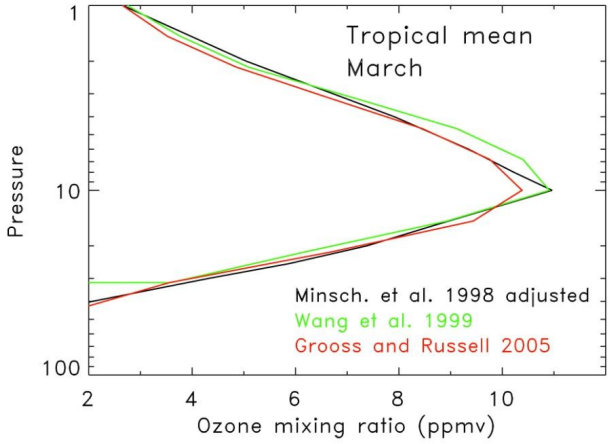

Fig. A1. Tropical (±10 degree latitude mean) ozone profiles for March from Minschwaner et al. (1998) (UARS MLS, March 1992–January 1993) in black, Wang et al. (1999) (UARS MLS, HALOE, and SAGE II, April 1992 March 1993) in green, and Grooß and Russell (2005) (UARS HALOE 1991–2002) in red. The profiles from Minschwaner et al. (1998) have been reduced by a constant 3 % to compensate for an overall positive bias with respect to the other datasets.

the vertical resolution of the retrievals is between 2 and 5 km. Uncertainties in ACE profile altitudes are 0.25 km, and no averaging kernels are considered for the error analysis as these are not available from the ACE trace gas retrievals (Boone et al., 2005).

Uncertainties in solar spectral irradiances, oxygen and ozone opacities, and in CFC cross sections will impact the calculated photolysis loss rate (Eq. 1). SORCE UV solar irradiances have mean accuracies of 3 % at wavelengths between 180 and 300 nm (McClintock et al., 2005), which translate into the same fractional uncertainties in lifetimes. There is an additional contribution to the lifetime uncertainty of 2 % due to solar variability effects. Similarly, fractional errors in CFC cross sections transfer directly to lifetime uncertainties. Absorption cross section uncertainties for CFC-11 and CFC-12 are both estimated to be 5 %, which is larger than the errors quoted by either Simon et al. (1988) or Merienne et al. (1990), but it is more consistent with the analysis presented in Sect. 2. Oxygen and ozone opacity uncertainties are more difficult to assess. Since vertical CFC profiles are fixed according to observations, reduced oxygen and ozone optical depths lead to increased J values and shorter lifetimes, while increased optical depths lead to longer lifetimes. For oxygen, the absorption cross section is the sole source of error in optical depth because oxygen column abundances can be specified exactly according to pressure. The combined uncertainty in O_2 S-R band line strengths and line wing cross sections is taken to be 10 %, while O_2 Herzberg continuum cross section uncertainties are similar in magnitude (Nicolet and Kennes, 1988). The Herzberg spectral region has more of an impact on CFC-11 relative to CFC-12, as expected from the spectral J values discussed in Sect. 2. The combined effects of considered errors in O_2 cross sections are on the order of 17 % for CFC-11 and 10 % for CFC-12 J values, which are larger than the cross section errors because of the amplifying effect of changes to the radiation field at large optical depths. Associated uncertainties in computed lifetimes range between 6 and 10 yr for CFC-11 and 10–11 yr for CFC-12 (Table A1).

Ozone optical depths contain two sources of error: one from the absorption cross section and another from the assumed ozone climatology. Below 225 nm, recent measurements of O_3 absorption cross sections agree to within 3–5 % (Sander et al., 2011) and we adopt a mean uncertainty of 3 %, which translates into uncertainties of 5 % and 3 % in computed photolysis rates for CFC-11 and CFC-12, respectively. Similar impacts on CFC J values are felt from uncertainties in the vertical, latitudinal, and seasonal ozone distributions. In general, reduced ozone concentrations lead to smaller optical depths at lower altitudes and shorter lifetimes, although with less ozone, the production of $O(^1D)$ is suppressed locally leading to less CFC destruction and a tendency towards longer lifetimes. Here, we consider uniform increases or decreases in tropical ozone (where most loss occurs, cf. Sect. 3). For ±3 % changes in ozone concentrations, the computed CFC lifetime changes were ±6 % for CFC-11 and ±3 % for CFC-12, respectively. Similar to the O_2 Herzberg cross sections, uncertainties in ozone have a larger relative impact on CFC-11 since its spectral J value emphasizes longer wavelengths where ozone opacity has a larger influence. The 3 % ozone uncertainty is based on variations seen between the low-latitude climatologies of Minschwaner et al. (1998), Wang et al. (1999), and Grooß and Russell (2005). Figure A1 shows an example of tropical mean profiles, where the Minschwaner et al. (1998) ozone has been uniformly decreased by 3 % in order to remove differences of this order of magnitude with the other two climatologies. The combined effect of ozone cross section and vertical profile uncertainties on CFC-11 and CFC-12 lifetimes are 2.9–4.8 yr and 4.7–4.8 yr, respectively.

There are, in addition, uncertainties in calculating $O(^1D)$ loss, global burdens (Eq. 3), and in converting transient

lifetimes to steady-state conditions. Uncertainties introduced in the calculation of $O(^1D)$ reactions are relatively small ($\sim 1\,\%$) due to a small relative contribution to the overall CFC loss. Uncertainties in global burdens arise primarily from estimating global mean tropospheric mixing ratios, which determine at least 80 % of the total atmospheric burden, along with the climatology of temperatures used to determine densities for conversion to absolute concentrations. Possible errors in mean mixing ratios and in the climatology of temperature combine to produce an uncertainty of 1.5 % in the global burden for both molecules. The conversion from transient to steady-state lifetime relies on knowledge of growth rates and the mean age of stratospheric air in the region of maximum loss, which have possible errors of $0.5\,\%\,yr^{-1}$ and 0.5 yr, respectively. These errors translate into mean uncertainty contributions of 0.6 yr and between 1.4 and 1.8 yr for steady-state lifetimes of CFC-11 and CFC-12, respectively.

While the values listed in Table A1 are given in years, the overall uncertainties given in Tables 1 and 2 were computed as percentages of the inverse lifetimes and combined using root-sum-square assuming independent contributions from each error source. The total error in inverse lifetime was then used to determine the minimum and maximum values of inverse lifetime and the corresponding range in lifetime for each dataset. For the best-estimate uncertainties, all of the errors were common to the datasets except for those associated with stratospheric profiles. Therefore, the common errors were combined and applied to the mean inverse lifetime, while the overall stratospheric profile error was obtained from the RSS of the individual profile errors and combined in quadrature with the total of the common errors. The maximum and minimum in best-estimate lifetime were computed from the range of mean inverse lifetimes.

Acknowledgements. This work was partially supported through NASA grant NNX08AN78G to New Mexico Tech. The ACE mission is supported primarily by the Canadian Space Agency. PFB and AB would also like to thank the UK Natural Environment Research Council (NERC) and the National Centre for Earth Observation (NCEO) for financial support. We thank Andreas Engel, Elliot Atlas, and Michael Volk for valuable advice and suggestions for this work.

Edited by: M. Palm

References

Amoruso, A., Crescentini, L., Cola, M. S., and Fiocco, G.: Oxygen absorption cross sections in the Herzberg continuum, J. Quant. Spectrosc. Radiat. Transf., 56, 145–152, 1996.

Brown, A. T., Chipperfield, M. P., Boone, C., Wilson, C., Walker, K. A., and Bernath, P. F.: Trends in atmospheric halogen containing gases since 2004, J. Quant. Spectrosc. Radiat. Transf., 112, 2552–2566, 2011.

Bernath, P. F., McElroy, C. T., Abrams, M. C., Boone, C. D., Butler, M, Camy-Peyret, C., Carleer, M., Clerbaux, C., Coheur, P. F., Colin, R., DeCola, P., DeMaziere, M., Drummond, J. R., Dufour, D., Evans, W. F. J., Fast, H., Fussen, D., Gilbert, K., Jennings, D. E., Llewellyn, E. J., Lowe, R. P., Mahieu, E., McConnell, J. C., McHugh, M., McLeod, S. D., Michaud, R., Midwinter, C., Nassar, R., Nichitiu, F., Nowlan, C., Rinsland, C. P., Rochon, Y. J., Rowlands, N., Semeniuk, K., Simon, P., Skelton, R., Sloan, J. J., Soucy, M. A., Strong, K., Tremblay, P., Turnbull, D., Walker, K. A., Walkty, I., Wardle, D. A., Wehrle, V., Zander, R., and Zou, J.: Atmospheric Chemistry Experiment (ACE): Mission overview, Geophys. Res. Lett, 32, L15S01, doi:10.1029/2005GL022386, 2005.

Boone, C. D., Nassar, R., Walker, K. A., Rochon, Y., McLeod, S. D., Rinsland, C. P., and Bernath, P. F.: Retrievals for the atmospheric chemistry experiment Fourier-transform spectrometer, Appl. Optics, 44, 7218–7231, 2005.

Brasseur, G. and Solomon, S.: Aeronomy of the Middle Atmosphere (3rd ed.), Springer, Dordrecht, 2005.

Crutzen, P. J. and Schmailzl, U.: Chemical budgets of the stratosphere, Planet. Space Sci., 31, 1009–1032, 1983.

Cunnold, D. M., Prinn, R. G., Rasmussen, R. A., Simmonds, P. G., Alyea, F. N., Cardelino, C. A., Crawford, A. J., Fraser, P. J., and Rosen, R. D.: The Atmospheric Lifetime Experiment 3. Lifetime Methodology and Application to Three Years of CFCl3 Data, J. Geophys. Res., 88, 8379–8400, 1983.

Cunnold, D. M., Prinn, R. G., Rasmussen, R. A., Simmonds, P. G., Alyea, F. N., Cardelino, C. A., Crawford, A. J., Fraser, P. J., and Rosen, R. D.: Atmospheric lifetime and annual release estimates for $CFCl_3$ and CF_2Cl_2 from 5 years of ALE data, J. Geophys. Res., 91, 797–817, 1986.

DeMore, W. B., Sander, S. P., Golden, D. M., Hampson, R. F., Kurylo, M. J., Howard, C. J., Ravishankara, A. R., Kolb, C. E., and Molina, M. J.: Chemical kinetics and photochemical data for use in stratospheric modeling, Evaluation 12, JPL Pub. 97-4, Jet Propulsion Laboratory, Pasadena, 1997.

Douglass, A. R., Stolarski, R. S., Schoeberl, M. R., Jackman, C. H., Gupta, M. L., Newman, P. A., Nielsen, J. E., and Fleming, E. L.: Relationship of loss, mean age of air, and the distribution of CFCs to stratospheric circulation and implications for atmospheric lifetimes, J. Geophys. Res., 113, D14309, doi:10.1029/2007JD009575, 2008.

Grooß, J.-U. and Russell III, James M.: Technical note: A stratospheric climatology for O_3, H_2O, CH_4, NO_x, HCl and HF derived from HALOE measurements, Atmos. Chem. Phys., 5, 2797–2807, doi:10.5194/acp-5-2797-2005, 2005.

Hoffmann, L., Spang, R., Kaufmann, M., and Riese, M.: Retrieval of CFC-11 and CFC-12 from Envisat MIPAS observations by means of rapid radiative transfer calculations, Adv. Space Res., 36, 915–921, 2005

Hoffmann, L., Kaufmann, M., Spang, R., Müller, R., Remedios, J. J., Moore, D. P., Volk, C. M., von Clarmann, T., and Riese, M.: Envisat MIPAS measurements of CFC-11: retrieval, validation, and climatology, Atmos. Chem. Phys., 8, 3671–3688, doi:10.5194/acp-8-3671-2008, 2008.

Jackman, C. H. and Guthrie, P. D.: Sensitivity of N_2O, $CFCl_3$, and CF_2Cl_2 two-dimensional distributions to O_2 absorption cross sections, J. Geophys. Res., 90, 3919–3923, 1985.

Johnston, H. S., Serang, O., and Podolske, J.: Instantaneous global nitrous oxide photochemical rates, J. Geophys. Res., 84, 5077–5082, 1979.

Ko, M. K. W. and Sze, N. D.: A 2-D model calculation of atmospheric lifetimes for N_2O, CFC-11 and CFC-12, Nature, 297, 317–319, 1982.

Ko, M. K. W., Sze, N. D., and Weisenstein, D. K.: Use of satellite data to constrain the model-calculated atmospheric lifetime for N_2O: Implications for other grace gases, J. Geophys. Res., 96, 7547–7552, 1991.

Kuell, V., Offermann, D., Jarisch, M., Schaeler, B., Engel, A., Claude, H., Smit, H. G. J., Ebel, A., and Feldmann, H.: Tropopause region temperatures and CFC 11 mixing ratios from CRISTA 2, J. Geophys. Res., 110, D16104, doi:10.1029/2004JD005592, 2005.

Lean, J.: Evolution of the sun's spectral irradiance since the Maunder Minimum, Geophys. Res. Lett., 27, 2425–2428, 2000.

Meier, R. R., Anderson, D. E., and Nicolet, M.: Radiation field in the troposphere and stratosphere from 240–1000 nm I. General analysis, Planet. Space Sci., 30, 923–933, 1982

Merienne, M. F., Coquart, B., and Jenouvrier, A.: Temperature effects on the ultraviolet absorption of $CFCl_3$, CF_2Cl_2, and N_2O, Planet. Space Sci., 38, 617–625, 1990.

Minschwaner, K., Anderson, G. P., Hall, L. A., and Yoshino, K: Polynomial coefficients for calculating O_2 Schumann-Runge cross sections at 0.5 cm^{-1} resolution, J. Geophys. Res., 97, 10103–10108, 1992.

Minschwaner, K., Salawitch, R. J., and McElroy, M. B.: Absorption of solar radiation by O_2: Implications for O_3 and lifetimes of N_2O, $CFCl_3$, and CF_2Cl_2, J. Geophys. Res., 98, 10543–10561, 1993.

Minschwaner, K.: High-resolution analysis of direct and scattered radiation in the stratosphere between 175 and 210 nm, J. Geophys. Res., 99, 3677–3684, 1994.

Minschwaner, K., Carver, R. W., Briegleb, B. P., and Roche, A. E.: Infrared radiative forcing and atmospheric lifetimes of trace species based on observations from UARS, J. Geophys. Res., 103, 23243–23253, 1998.

Newman, P. A., Daniel, J. S., Waugh, D. W., and Nash, E. R.: A new formulation of equivalent effective stratospheric chlorine (EESC), Atmos. Chem. Phys., 7, 4537–4552, doi:10.5194/acp-7-4537-2007, 2007.

Nicolet, M. and Kennes R.: Aeronomic problems of the molecular oxygen photodissociation, IV: The various parameters for the Herzberg continuum, Planet. Space Sci., 36, 1069–1076, 1988.

Nightingale, R. W., Roche, Q. E., Kumer, J. B., Mergenthaler, J. L., Gille, J. C., Massie, S. T., Bailey, P. L., Edwards, D. P., Gunson, M. R., Toon, G. C., Sen, B., Blavier, J.-F., and Connell, P. S.: Global CF_2Cl_2 measurements by UARS cryogenic limb array etalon spectrometer: Validation by correlative data and a model, J. Geophys. Res., 101, 9711–9736, 1996.

Plumb, R. A. and Ko, M. K. W.: Interrelationships between mixing ratios of long lived stratospheric constituents, J. Geophys. Res., 97, 10145–10156, 1992.

Riese, M., Sprang, R., Preusse, P., Ern, M., Jarisch, M., Offerman, D., and Grossmann, K. U.: Cryogenic Infrared Spectrometers and Telescopes for the Atmosphere (CRISTA) data processing and atmospheric temperature and trace gas retrieval, J. Geophys. Res., 104, 16349–16367, 1999.

Rottman, G. J., Woods, T. N., and McClintock, W.: SORCE Solar UV Irradiance Results, Adv. Space Res., 37, 201–208, doi:10.1016/j.asr.2005.02.072, 2006.

Sander, S. P., Abbatt, J., Barker, J. R., Burkholder, J. B., Friedl, R. R., Golden, D. M., Huie, R. E., Kolb, C. E., Kurylo, M. J., Moortgat, G. K., Orkin V. L., and Wine P. H.: Chemical Kinetics and Photochemical Data for Use in Atmospheric Studies, Evaluation No. 17, JPL Publication 10-6, Jet Propulsion Laboratory, Pasadena, http://jpldataeval.jpl.nasa.gov, 2011.

Schoeberl, M. R., Douglass, A. R., Stolarski, R. S., Pawson, S., Strahan, S. E., and Read, W.: Comparison of lower stratospheric tropical mean vertical velocities, J. Geophys. Res., 113, D24109, doi:10.1029/2008JD010221, 2008.

Simon, P. C., Gillotay, G., Vanlaethem-Meuree, N., and Wisemberg, J.: Ultraviolet absorption cross-sections and chloro and chlorofluoro-methanes at stratospheric temperatures, J. Atmos. Chem., 7, 107–135, 1988.

Volk, C. M., Elkins, J. W., Fahey, D. W., Dutton, G. S., Gilligan, J. M., Loewenstein, M., Podolske, J. R., Chan, K. R., and Gunson, M. R.: Evaluation of source gas lifetimes from stratospheric observations, J. Geophys. Res., 102, 25543–25564, 1997.

Wang, H. J., Cunnold, D. M., Froidevaux, L., and Russell, J. M.: A reference model for middle atmosphere ozone in 1992–1993, J. Geophys. Res., 104, 21629–21643, 1999.

WMO (World Meteorological Organization): Scientific Assessment of Ozone Depletion: 2010, Global Ozone Research and Monitoring Project – Report No. 52, 516 pp., Geneva, Switzerland, 2011.

Wofsy, S. C., McElroy, M. B., Sze, N. D.: Freon consumption: Implications for atmospheric ozone, Science, 187, 535–537, 1975.

Yoshino, K., Cheung, A. S.-C., Esmond, J. R., Parkinson, W. H., Freeman, D. E., and Guberman, S. L.: Improved absorption cross sections of oxygen in the wavelength region 205–240 nm of the Herzberg continuum, Planet. Space Sci., 36, 1469–1475, 1988.